Ab initio refinement of the thermal equation of state for bcc tantalum: the effect of bonding on anharmonicity

2009 J. Phys.: Condens. Matter 21 095408

(http://iopscience.iop.org/0953-8984/21/9/095408)

J. Phys.: Condens. Matter **21** (2009) 095408 (10pp) doi:10.1088/0953-8984/21/9/095408

Ab initio refinement of the thermal equation of state for bcc tantalum: the effect of bonding on anharmonicity

Zhong-Li Liu[1,2], **Ling-Cang Cai**[1], **Xiang-Rong Chen**[2,3], **Qiang Wu**[1] **and Fu-Qian Jing**[1,2]

[1] Laboratory for Shock Wave and Detonation Physics Research, Institute of Fluid Physics, PO Box 919-102, 621900 Mianyang, Sichuan, People's Republic of China
[2] Institute of Atomic and Molecular Physics, College of Physical Science and Technology, Sichuan University, Chengdu 610065, People's Republic of China
[3] International Centre for Materials Physics, Chinese Academy of Sciences, Shenyang 110016, People's Republic of China

Received 28 October 2008, in final form 12 January 2009
Published 4 February 2009
Online at stacks.iop.org/JPhysCM/21/095408

Abstract

We report a detailed *ab initio* study for body-centered-cubic (bcc) Ta within the framework of the quasiharmonic approximation (QHA) to refine its thermal equation of state and thermodynamic properties. Based on the excellent agreement of our calculated phonon dispersion curve with experiment, the accurate thermal equations of state and thermodynamic properties are well reproduced. The thermal equation of state (EOS) and EOS parameters are considerably improved in our work compared with previous results by others. Furthermore, at high temperatures, the excellent agreement of our obtained thermal expansion and Hugoniot curves with experiments greatly verifies the validity of the quasiharmonic approximation at higher temperatures. It is known that pressure suppresses the vibrations of atoms from their equilibrium positions, i.e. the bondings among atoms are strengthened by pressure; for the same temperature, anharmonicity becomes less important at high pressure. Thus the highest valid temperature of the QHA can be reasonably extended to the larger range.

(Some figures in this article are in colour only in the electronic version)

1. Introduction

Tantalum, a d-band metal, is a very useful pressure standard and high technology material owing to its high chemical and mechanical stability, large isothermal compressibility and high melting point (3269 K). Because of its important position in the field of material science and condensed matter science, it has recently attracted tremendous experimental and theoretical interest in its wide range of properties including the equation of state (EOS) [1–4], the elastic [1, 5, 6], lattice dynamical [6–8] and melting properties [7–13], etc. The phase diagram and melting properties of Ta have greatly challenged the methods of experiments and theories in the past decade [13].

As some of the very fundamental properties, the accurate thermal equation of state (EOS) and thermodynamic properties as a function of pressure and temperature can directly provide valuable information for understanding the phase diagram and dynamical response of materials under extreme conditions. The thermal EOS is a measure of the relationship between pressure, volume and temperature (P–V–T). The inclusion of temperature makes it more important than the P–V equation of state. Even though many theoretical calculations [1, 7, 8, 11–13] have been performed on its EOS, it is important that the complete thermal EOS and thermodynamic properties of Ta should be further refined theoretically. Earlier, Cohen and Gülseren [1] applied the particle-in-cell (PIC) model and obtained the thermal equation of state, but their thermal expansion and heat capacity are relatively far from experiments. The PIC model they used has been questioned when it is applied at high pressure and temperature [14]. So the accurate complete thermal equation of state should be determined with more accurate theoretical methods.

In this paper, we apply the quasiharmonic approximation to the study of the lattice dynamical properties, the thermal EOS and thermodynamic properties of Ta. Density functional

perturbation theory (DFPT) is a well-established method for calculating the vibrational properties from first principles in the framework of the quasiharmonic approximation. The crystal free energy is easily included by adding the phonon free energy to the static energy through the standard density functional (DFT) theory calculations. Including the part anharmonic effects play by considering the volume dependence of phonon frequencies gives access to thermal expansion, the thermal EOS and thermodynamic properties.

At ambient conditions, Ta is a body-centered-cubic (bcc) structure. The diamond-anvil cell (DAC) experiment [2] indicated the bcc structure remains stable up to 174 GPa. Furthermore shock wave (SW) experiments [15–17] and theoretical calculations [11, 18] indicated that the bcc phase continues to be stable under pressure up to 500 GPa. So, in this work, we treat bcc as the unique phase of Ta at high pressure and high temperature.

This paper is organized as follows. In section 2, we give a detailed description of the method of first-principles calculations and the technical details. The results and detailed discussions are presented in section 3. Section 4 is a summary of the results and a general conclusion.

2. Computational details

Within the quasiharmonic approach (QHA), the Helmholtz free energy of metal at constant volume V and temperature T is given by

$$F(V,T) = F_{\rm el}(V,T) + F_{\rm zp}(V,T) + F_{\rm ph}(V,T), \quad (1)$$

where $F_{\rm el}(V,T)$ is the electronic free energy directly obtained from the total energy calculations, from which the electronic free energy of the metal due to thermal electronic excitations can be included using the standard methods of finite-temperature DFT developed by Mermin [19]. $F_{\rm el}(V,T)$ is written as

$$F_{\rm el}(V,T) = E_{\rm el}(V,T) - TS_{\rm el}(V,T). \quad (2)$$

The electronic entropy is given by

$$S_{\rm el}(V,T) = -2k_{\rm B}\sum_i f_i \ln f_i + (1-f_i)\ln(1-f_i), \quad (3)$$

where $k_{\rm B}$ is Boltzmann's constant and f_i is the Fermi–Dirac occupation number of orbit i.

The second term of equation (1) is the zero-point motion energy given by $F_{\rm zp} = \frac{1}{2}\sum_{\mathbf{q},j}\hbar\omega_j(\mathbf{q},V,T)$. The last term is the phonon free energy arising from the lattice vibrations, which is obtained from

$$F_{\rm ph}(V,T) = k_{\rm B}T\sum_{\mathbf{q},j}\ln\{1-\exp(-\hbar\omega_j(\mathbf{q},V,T)/k_{\rm B}T)\}, \quad (4)$$

where $\omega_j(q,V,T)$ is the phonon frequency of the jth mode at wavevector $\mathbf{q}$ in the Brillouin zone (BZ). The phonon frequencies slightly depend on temperature due to electronic excitations for transition metals, but the normal quasiharmonic approach does not cause any serious problems to the results [20, 21] and we neglected this dependence in this work.

The vibrational frequencies of Ta were determined at 18 volumes within the framework of the density functional perturbation theory (DFPT) [22, 23]. Our calculations were performed within the generalized gradient approximation (GGA) to density functional theory, as implemented in the QUANTUM-ESPRESSO package [23]. A nonlinear core correction to the exchange–correlation energy function was introduced to generate a Vanderbilt ultrasoft pseudopotential for Ta with the valence electrons' configuration of $5s^25p^66s^25d^3$. In addition, the pseudopotential was generated with a scalar-relativistic calculation using GGA according to the recipe of Perdew–Burke–Ernzerhof (PBE) [24].

We made careful tests on $\mathbf{k}$ and $\mathbf{q}$ grids, the kinetic energy cutoff and many other parameters to guarantee phonon frequencies and free energies to be well converged. Dynamical matrices were computed at 29 wave ($\mathbf{q}$) vectors using an $8\times8\times8$ $\mathbf{q}$ grid in the irreducible wedge of the Brillouin zone. The kinetic energy cutoff $E_{\rm cutoff}$ was 60 Ryd and the $\mathbf{k}$ grids used in both total energy and phonon calculations were $24\times24\times24$ Monkhorst–Pack (MP) [25] meshes. The self-consistent calculation was terminated when the total energy difference in two successive loops was less than 10^{-12} Ryd. A Fermi–Dirac smearing width of 0.01 Ryd was applied for Brillouin zone integrations in phonon frequency calculations, and in the calculations of static energy and thermal electronic excitations we treated the smearing width of Fermi–Dirac as the physical temperature of electrons. Different smearing widths can all make the total energy to be well converged in the large enough $24\times24\times24$ MP k-meshes. The geometric mean phonon frequency $\overline{\omega}$ is defined by

$$\ln\overline{\omega} = \frac{1}{N_{\mathbf{q}j}}\sum_{\mathbf{q}j}\ln\overline{\omega_{\mathbf{q}j}} \quad (5)$$

where $\omega_{\mathbf{q}j}$ is the phonon frequency of branch j at wavevector $\mathbf{q}$ and $N_{\mathbf{q}j}$ is the number of branches times the total number of $\mathbf{q}$ points in the sum. With the tested parameters, the geometric mean phonon frequency $\overline{\omega}$ was converged to 0.5 $\rm cm^{-1}$. Within the framework of the density functional perturbation theory (DFPT), a unit cell is used for calculating phonon dispersion curves. Figure 1 shows the obtained dispersion curves at zero pressure along several high-symmetry directions in the BZ for both transverse (TA) and longitudinal (LA) acoustical branches. One finds excellent agreement of the dispersion curves with the neutron diffraction experiment [26]. We repeated the phonon calculations for another 17 different volumes, from which we obtained the phonon free energy according to equation (4). Some of the dispersion curves corresponding to volumes from 18.47 to 6.75 $\rm Å^3$ are plotted in figure 2, which shows the well-known phenomenon in solids, i.e. the phonon frequencies increase as volume decreases.

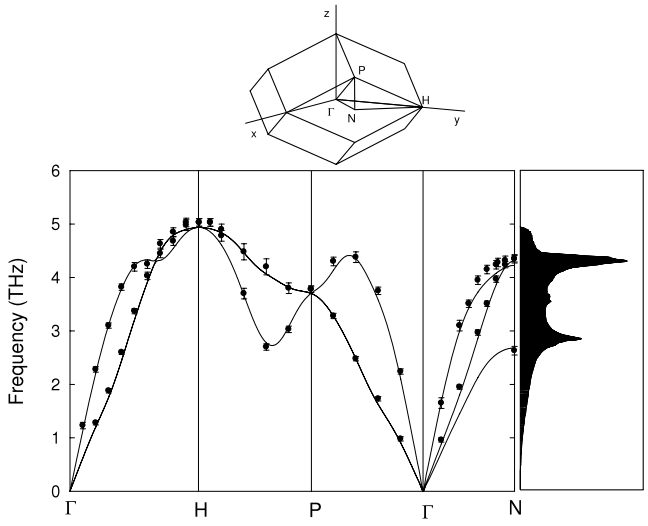

Figure 1. Phonon dispersion curves of bcc Ta at zero pressure. The solid circles with error bars are neutron diffraction experimental data [26]. The first Brillouin zone of bcc Ta is plotted on the top. The phonon density of states is also shown on the right-hand side.

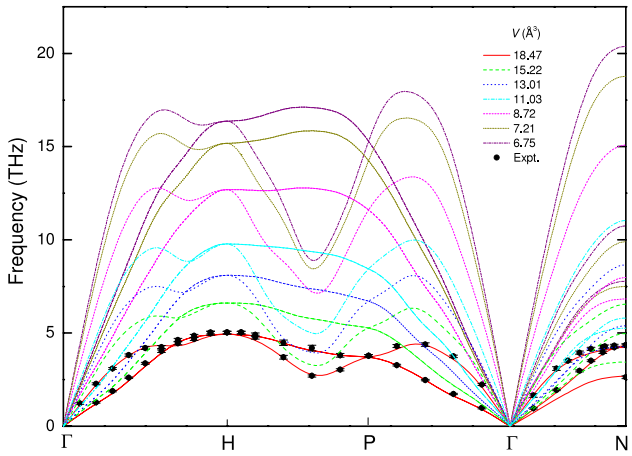

Figure 2. Some of the obtained phonon dispersion curves at volumes from 18.47 to 6.75 Å^3. It is shown that the phonon frequencies increase with increasing pressure. The solid circles with error bars are neutron diffraction experimental data [26].

3. Results and discussions

3.1. Thermal equation of state

We obtained the Helmholtz free energy as a function of volume V and temperature T from equation (1). Figure 3 shows the Helmholtz free energy as a function of volume at temperatures from 0 to 4000 K. The thermal EOS and its parameters are then derived by fitting a fifth-order finite strain equation of state (EOS) [27] to the free energy versus volume at each temperature. The calculated isothermal compressional curves are compared with experiments [2–4] in figure 4. From figure 4, one notes the 0 K isotherm (including zero-point motion) is almost the same as the 300 K one and this is due to the small free energy contribution from the lattice vibrations at 300 K, while, when the temperature goes from 300 to

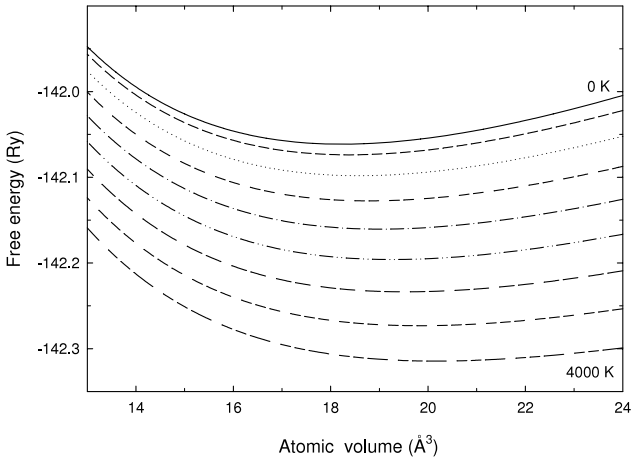

Figure 3. The free energy versus volume curves of bcc Ta at temperatures from 0 to 4000 K with 500 K intervals.

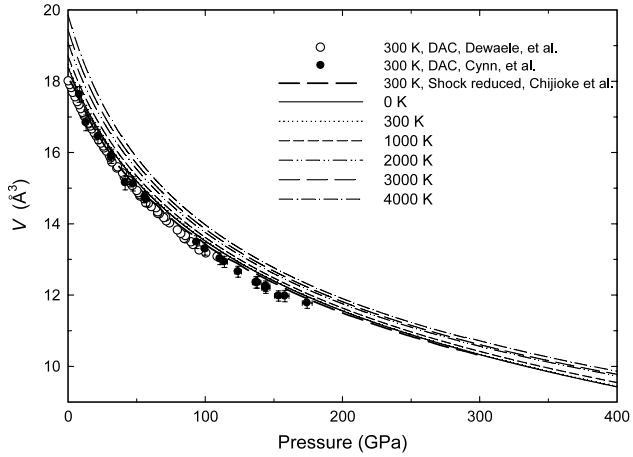

Figure 4. Isotherms of bcc Ta at different temperatures, compared with room temperature experimental data [2–4].

Table 1. The fifth-order finite strain equation of state parameters. Experimental data are from [3].

	V_0 (Å^3)	K_0 (GPa)	K_0'
300 K	18.470	194.4	3.06
Expt. [3]	18.035	194	3.52

4000 K, the contribution of the phonon free energy becomes larger and larger. Our 300 K isotherm deviates from DAC experimental data with increasing pressure, but the agreement with the shock-reduced isotherm [4] is reasonably good. We show finite strain EOS fitting parameters, $F_0(T)$, $V_0(T)$ and $K_0(T)$ as functions of temperature in figure 5 and table 1. The agreement of our results of the equilibrium volume V_0 and bulk modulus K_0, and K_0' with experimental data is very good.

According to standard thermodynamic relations, the pressure P is written as

$$P = -\left.\frac{\partial F}{\partial V}\right|_T. \tag{6}$$

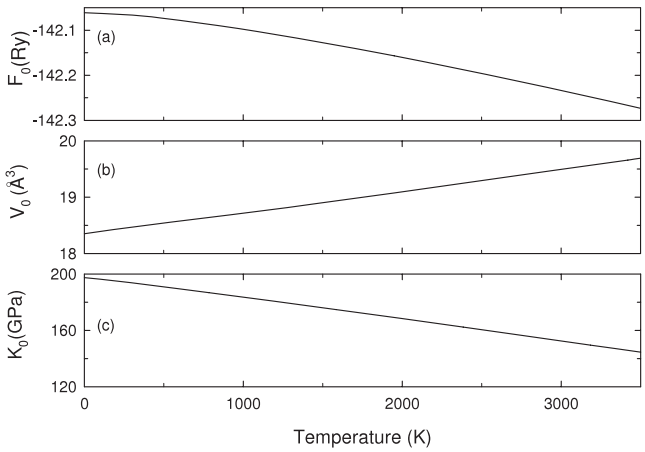

Figure 5. Fitted finite strain equation of state parameters: (a) $F_0(T)$, (b) $V_0(T)$, (c) $K_0(T)$ as functions of temperature.

From equations (1) and (6) we obtained

$$P = P_{\rm el} + P_{\rm zp} + P_{\rm ph}. \tag{7}$$

Thermal pressure is induced by increasing the temperature at constant volume, so we write thermal pressure as $P_{\rm th} = P_{\rm el} + P_{\rm ph}$. As described above, here we neglected the dependences of phonon frequencies on temperature, so $P_{\rm zp}$ is independent of temperature. In figure 6, we plotted the deduced thermal pressure as a function of volume and temperature. From figure 6(a), one notes that the thermal pressure decreases with increasing volume and shows the monotonic behavior. This is different from the results of Cohen and Gülseren via the particle-in-cell (PIC) model [1], which showed the thermal pressures first decrease with decreasing volume, and then present a minimum at a certain compression. As far as the non-monotonic behavior of the thermal pressure is concerned, Cohen and Gülseren attributed to the fit to the electronic topological transition and thus the inflexibility in the fitted Vinet equation of state. As for the temperature dependence of thermal pressure (figure 6(b)), all the lines are quite linear, with slopes varying from 0.0026 to 0.0167 GPa K^{-1}. This is also different from the results obtained by Cohen and Gülseren, which indicate the lines have the same constant slope of 0.004 42 GPa K^{-1} for almost all volumes [1].

Our obtained thermal pressures of Ta are much larger than the DAC values [10] which are generally not more than 2 GPa over the wide range of pressure and temperature. The large deviation of our results from the DAC experiment can be partly attributed to the fact that the thermal pressure of the DAC experiment [10] is calculated by assuming the thermal pressure of room temperature is 0, while we calculated the thermal pressure from 0 K and included the very important contribution arising from electronic excitation [28, 29]. Our thermal pressures of Ta are comparable with those of hexagonal-close-packed (hcp) Fe which also has very large thermal pressure at the similar high pressures and temperatures [29]. Except for Fe, the experiments and calculations both indicated that MgO [30, 31] and $MgSiO_3$ [31, 32] also showed considerable thermal pressure (more than 10 GPa at ∼2000 K and equilibrium volume) at high P–Ts.

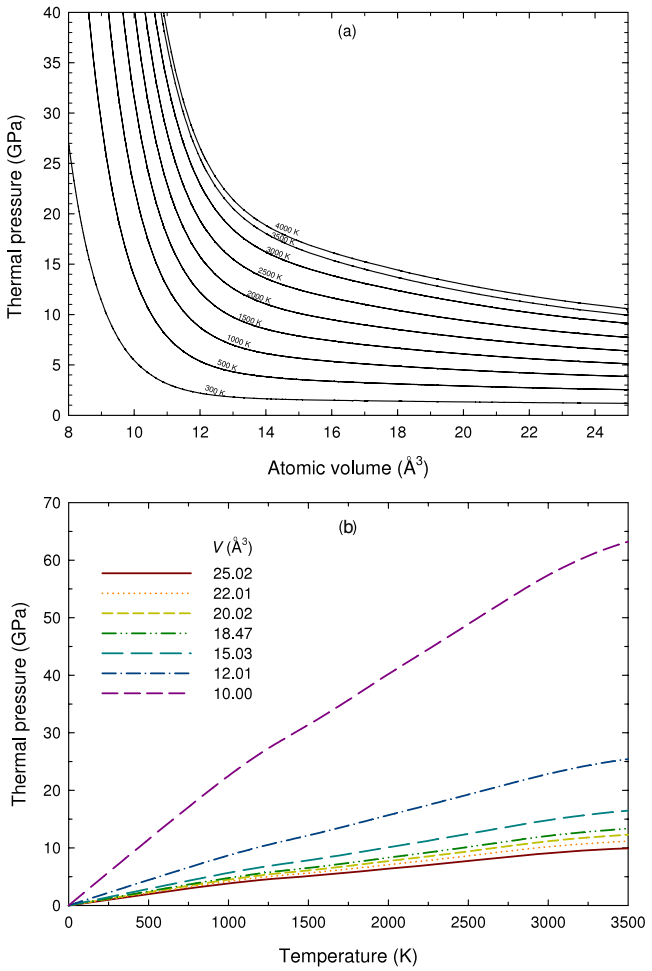

Figure 6. The thermal pressure as a function of volume (a) and temperature (b). (a) Lines correspond to different temperatures. (b) Lines represent different volumes.

At equilibrium volume V_0 (18.47 $Å^3$), we separated the thermal pressure into two parts, electronic and vibrational. Figure 7 shows the electronic and vibrational thermal pressure as a function of temperature at V_0. The electronic thermal pressure is very little at low temperature, but it is larger and larger with increasing temperature and its weight increases from 0% to around 12% of total thermal pressure when the temperature goes up to 3000 K. Our calculated electronic thermal pressure is also comparable with those of Au and Pt obtained via the full-potential linear muffin-tin-orbital (FP-LMTO) method [21] and that of hcp Fe from the pseudopotential plane-wave method [28].

The Hugoniot curve is one of the fundamental properties of materials, which can reflect the response of the material to both pressure and temperature. We obtained Hugoniot curves according to the Rankine–Hugoniot formula:

$$U_{\rm H} - U_0 = \tfrac{1}{2}\,(P_{\rm H} + P_0)\,(V_0 - V_{\rm H}) \tag{8}$$

where $U_{\rm H}$, $P_{\rm H}$ and $V_{\rm H}$ are the molar internal energy, pressure and volume along the Hugoniot curve, respectively, and U_0 and V_0 are the molar internal energy and volume at pressure P_0 and room temperature. We obtained the pressure–volume

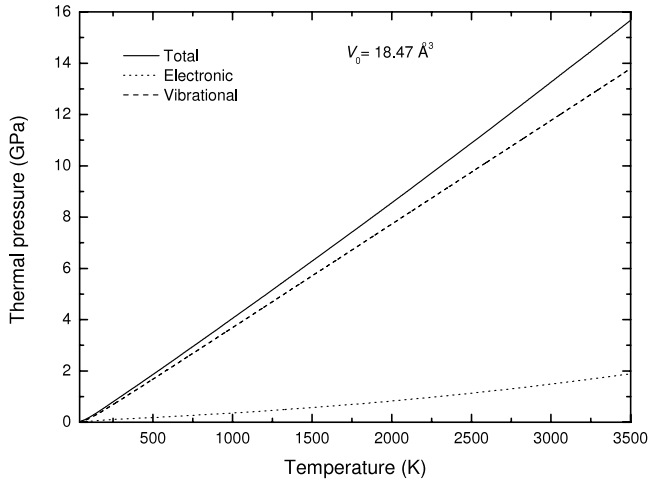

Figure 7. Thermal pressure as a function of temperature at $V_0 = 18.47$ Å^3. The electronic and lattice vibrational thermal pressures are separated.

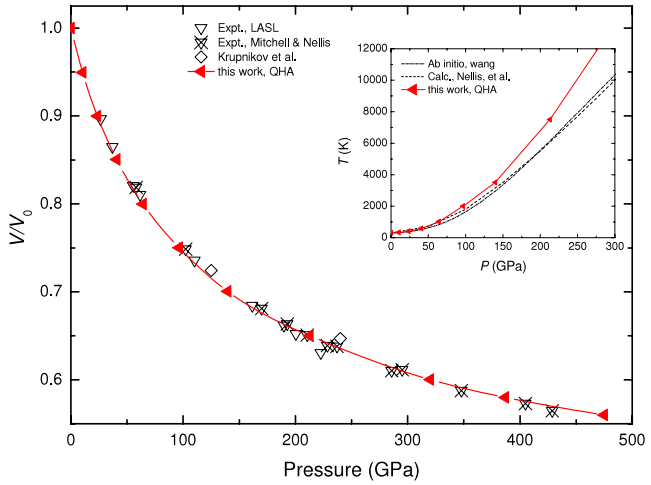

Figure 8. The volume–pressure and temperature–pressure (the inset) relations on Hugoniot curves obtained from the QHA, in comparison with experimental data [16, 33] and other calculations [17, 34].

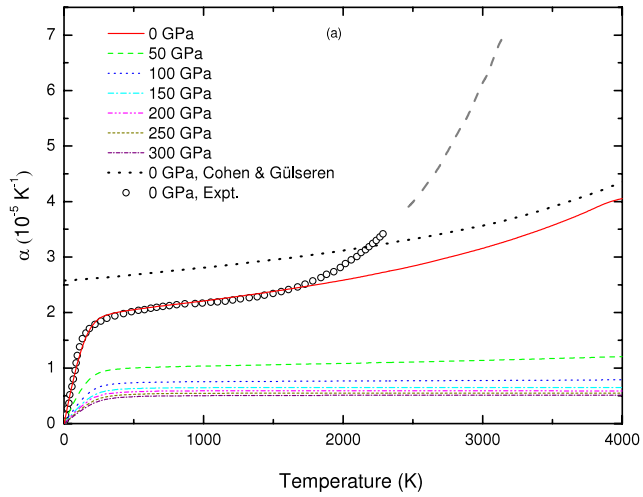

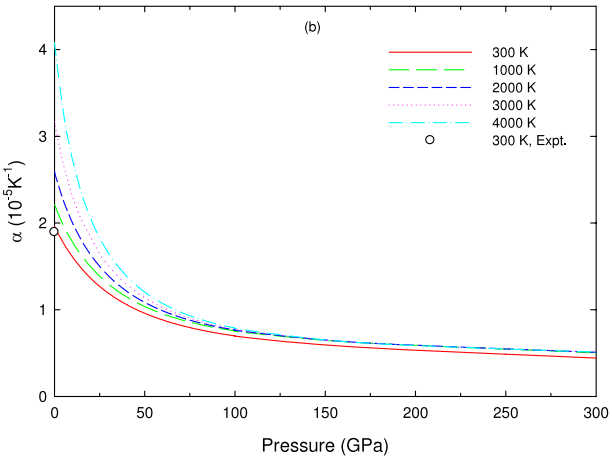

Figure 9. The thermal expansion coefficient as a function of (a) temperature and (b) pressure. Our zero-pressure results are in excellent agreement with experimental data [35]. (a) The thermal expansion coefficient versus temperature at different pressures. (b) The thermal expansion coefficient as a function of pressure at various temperatures. Also shown are the zero-pressure results from [1].

and temperature–pressure relations along the Hugoniot curve according to equation (8). Figure 8 shows the obtained Hugoniot curve of P–V and P–T. Our obtained Hugoniot curves are in excellent agreement with experiments [16, 33] and other calculations. The agreement of our P–T curve with other calculations is good below 150 GPa, but above 150 GPa other theoretical results deviate [17, 34] from our calculations.

3.2. Thermodynamic properties

The volume thermal expansion coefficient α_V can be derived via

$$\alpha_v = \frac{1}{V}\left(\frac{\partial V}{\partial T}\right)_P. \tag{9}$$

In figure 9, we plotted the thermal expansion coefficient as a function of P and T. Our zero-pressure results accord excellently with experimental data [35] in the low temperature region (figure 9(a)). The zero-pressure results of Cohen and Gülseren from the PIC model are also shown, but the agreement of our results with experiment seems better. Furthermore, our results reflect the continuous increase of thermal expansion coefficient when T goes from 0 to 300 K, but the calculations of Cohen and Gülseren do not. When the temperature is above 1700 K, our zero-pressure thermal expansion coefficient gradually deviates from experiments: this can be attributed to neglecting the other part of anharmonicity in our present calculations (see the discussions below). It is noted that the thermal expansion coefficient drops rapidly and its temperature dependence decreases with increasing pressure (figure 9(b)).

The linear thermal expansivity was obtained using $(a - a_0)/a_0$, where a_0 is the lattice constant at 0 K. In figure 10, we plot the lattice constant and the linear thermal expansion coefficient as a function of temperature and one notes the agreement of the linear thermal expansion coefficient with experiment [36] is very good.

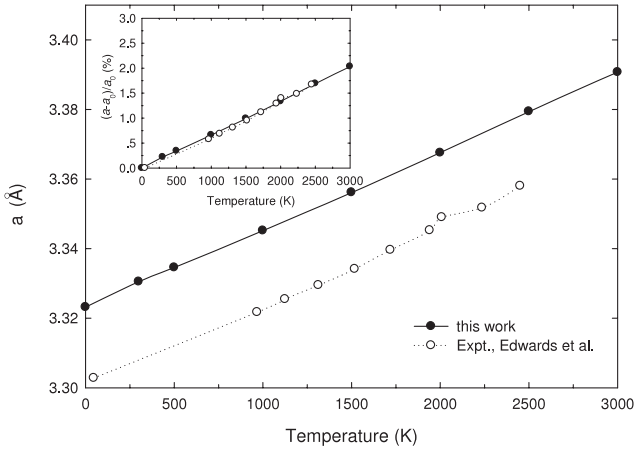

Figure 10. The lattice constant and linear thermal expansion coefficient (inset) as a function of temperature. Experimental data are from [36].

The specific heat at constant volume is defined by

$$C_V = \left(\frac{\partial U}{\partial T}\right)_V \tag{10}$$

where U is the internal energy of the system. C_P is different from C_V due to the thermal expansion caused by anharmonic effects. The relationship between C_P and C_V is determined by

$$C_P - C_V = \alpha_V^2(T) K_0 V T \tag{11}$$

where α_V is the volume thermal expansion coefficient, K_0 the bulk modulus, V the volume and T temperature. In figure 11, we plot C_V as a function of temperature and pressure. C_V increases dramatically as pressure increases and finally approaches a constant $3R$ (figure 11(a)). C_V as a function of pressure at fixed temperature is linear and the difference between isotherms at temperatures beyond 2000 K is quite small (figure 11(b)).

From equation (11), we obtained C_P as a function of temperature and pressure, which are compared with experimental data [37] and the 0 GPa results by Cohen and Gülseren [1] in figure 12. Our 0 GPa results agree better with experiment and they are in good accordance with experiments below 500 K but diverge from experiments beyond 500 K (figure 12(a)). C_P drops rapidly and its temperature dependence decreases with increasing pressure (figure 12(b)).

The thermodynamic Grüneisen parameter is a very important parameter through which the thermal pressure is related to the increase of thermal energy in the Mie–Grüneisen equation of state and it is defined by

$$\gamma = V\left(\frac{\partial P}{\partial U}\right)_V = \frac{\alpha K_T V}{C_V}, \tag{12}$$

where U is the internal energy. Our calculated zero-pressure 300 K value of γ is 1.75, very close to the experimental zero-pressure room temperature value of γ (1.65). As shown in figure 13(a), γ shows very weak dependence on temperature

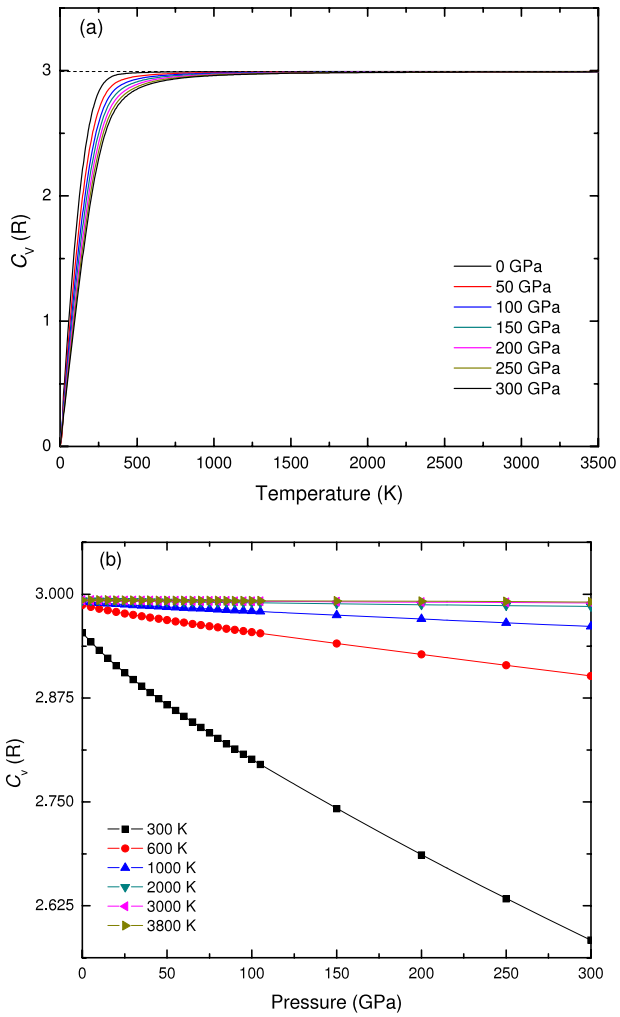

Figure 11. The specific heat capacity at constant volume as a function of (a) temperature and (b) pressure. (a) C_V as a function of temperature at different pressures. (b) C_V as a function of pressure at various temperatures.

along the isobar; however, its pressure dependence is strong (figure 13(b)) and it drops quickly as pressure increases. The behavior of our calculated γ with temperature and pressure is similar to that of Cohen and Gülseren [1] and that of Taioli *et al* [8].

The mode Grüneisen parameter $\omega_j(q)$ is defined by

$$\gamma_j(q) = -\frac{V}{\omega_j(q)}\frac{\partial \omega_j(q)}{\partial V}, \tag{13}$$

which expresses the volume dependence of the frequency of the jth vibration mode of the lattice. The dispersion curves of the mode Grüneisen parameters at zero pressure are shown in figure 14. The mode Grüneisen parameters are positive throughout the whole BZ for all three branches, indicating that there is no anomalous negative expansion.

The isothermal bulk modulus K_T can be obtained from

$$K_T = \frac{1}{\alpha}\left(\frac{\partial P}{\partial T}\right)_V. \tag{14}$$

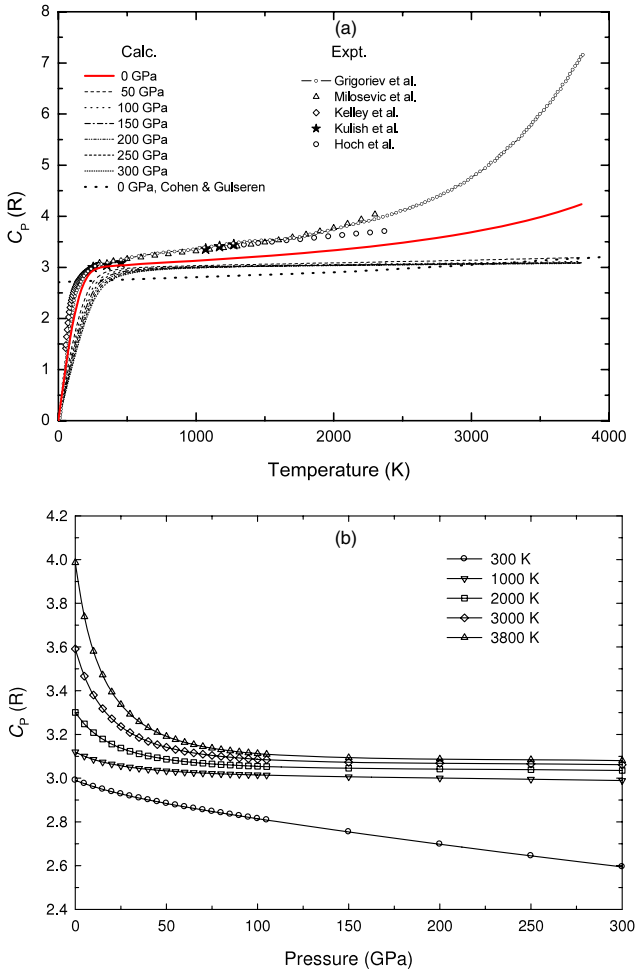

Figure 12. C_P as a function of (a) temperature and (b) pressure. (a) The lines correspond to different pressures. Experimental data are from [37]. Also shown are the 0 K results of Cohen and Gülseren. (b) C_P versus pressure at different temperatures.

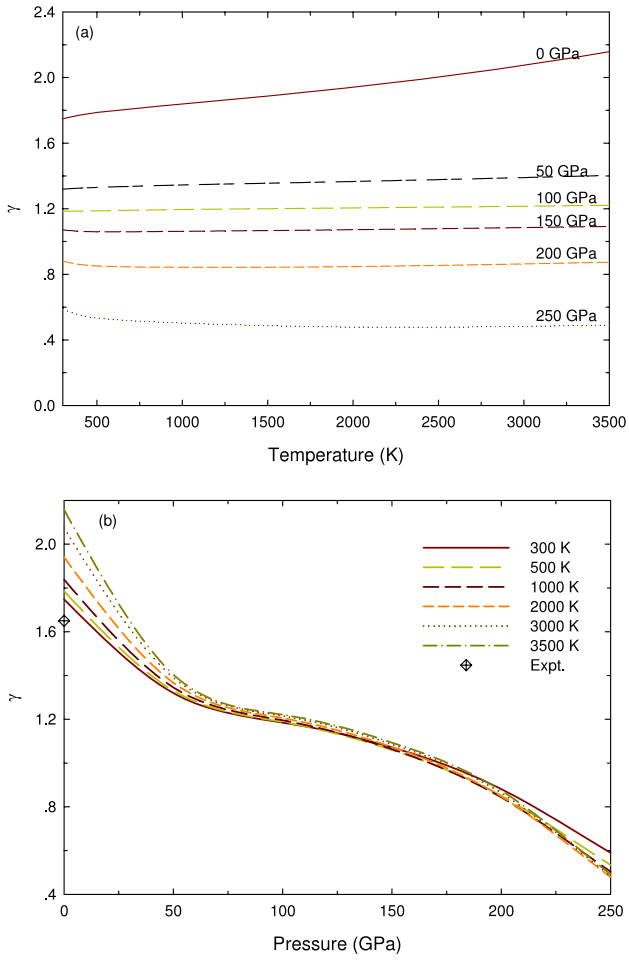

Figure 13. Variation of the Grüneisen parameter γ with (a) temperature and (b) pressure. The temperature dependence is moderate.

The adiabatic bulk modulus K_S correlates with K_T via

$$K_S - K_T = -\alpha\gamma K_T T. \tag{15}$$

Figures 15 and 16 show the isothermal and adiabatic bulk modulus as a function of temperature and pressure, respectively. The two moduli both decrease with increasing temperature at fixed pressures and increase with increasing pressure at different temperatures. The temperature dependence of the two moduli becomes weaker and weaker with increasing pressure.

Within the Debye approximation, the so-called Debye frequency is determined from the condition of the total number of modes to be equal to $3N$ for all acoustic branches:

$$3N = \int_0^{\omega_D} g(\omega)\,\mathrm{d}\omega, \tag{16}$$

where N is the number of atoms in the unit cell and $g(\omega)$ is the phonon density of states defined by

$$g(\omega) = \sum_{\mathbf{q},j} \delta\left[\omega - \omega_j(q)\right]. \tag{17}$$

So, according to the Debye model all the values of $\mathbf{q}$ are confined in a sphere with radius q_D. Usually, the Debye temperature is introduced as

$$\Theta_D = \frac{\hbar\omega_D}{k_B} \tag{18}$$

where $\hbar$ is Planck's constant and k_B is Boltzmann's constant. From equation (17), we can obtain the Debye temperature at 0 K.

According to the Debye approximation, the Helmholtz free energy at low temperature is

$$F = E_{\text{static}} + RT\left[\frac{9}{8}\left(\frac{\Theta_D}{T}\right) + 3\ln\left(1 - \mathrm{e}^{-\Theta_D/T}\right) - D\left(\frac{\Theta_D}{T}\right)\right], \tag{19}$$

$D(\Theta_D/T)$ is the Debye function written as

$$D\left(\frac{\Theta_D}{T}\right) = 3\left(\frac{T}{\Theta_D}\right)^3 \int_0^{\Theta_D/T} \frac{z^3\,\mathrm{d}z}{\mathrm{e}^z - 1}. \tag{20}$$

We obtained $\Theta_D(T)$ at temperature T by solving equation (19). Our results for the Debye temperature are displayed in figure 17. The zero-pressure 300 K result (Θ_D = 220 K) is

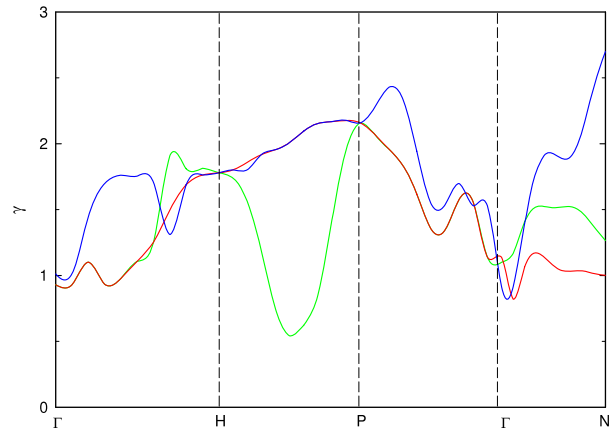

Figure 14. Mode Grüneisen parameters at zero pressure. The three lines (color online) correspond to three acoustic branches.

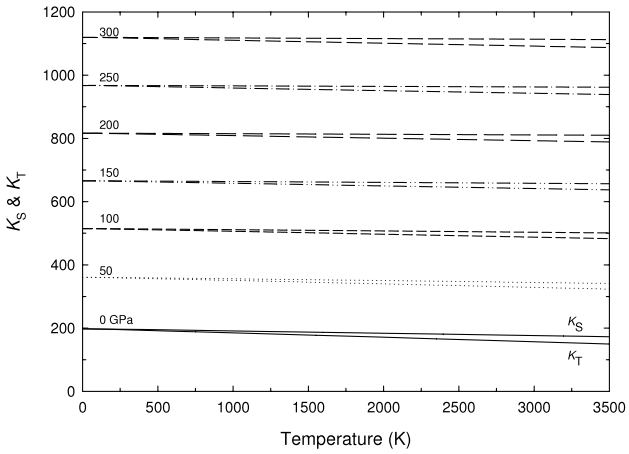

Figure 15. The adiabatic bulk modulus and isothermal bulk modulus versus temperature at different pressures. The lines correspond to the pressure from 0 to 300 GPa, and K_S is somewhat larger than K_T in each set of data at the same pressure.

in very good agreement with the experimental datum (Θ_D = 229 K) [38] derived from the standard entropy at 298 K and 0 GPa. $\Theta_D(T)$ shows a significant increase as pressure increases (decrease of volume). Firstly, $\Theta_D(T)$ drops with increasing T up to ∼70 K at fixed volume; however, in the temperature range from around 70 to 100 K, $\Theta_D(T)$ shows a moderate increase. Finally, with a further increase of T (above 200 K), it shows a weak temperature dependence.

3.3. The effect of bonding on anharmonicity

In this work, we constrained our calculations to the quasiharmonic approximation (QHA), and in the quite large range of temperatures it is valid, i.e. when the temperature is far from the melting point, part of the anharmonicity can be neglected reasonably. However, in fact the QHA includes the other part of anharmonicity by allowing phonon frequencies to vary with crystal volume (figure 2), but it ignores the change of electronic structure with increasing temperature and the effects on the lattice dynamical properties. Furthermore, in

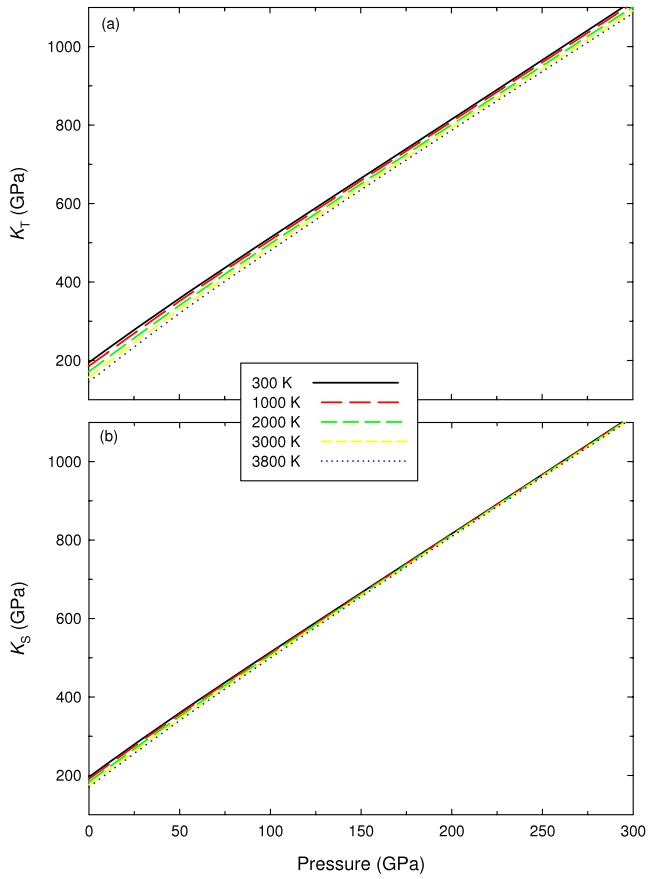

Figure 16. The isothermal bulk modulus and adiabatic bulk modulus versus pressure at different temperatures. (a) The isothermal bulk modulus variation with pressure at several temperatures. (b) The variation of adiabatic bulk modulus with pressure at various temperatures.

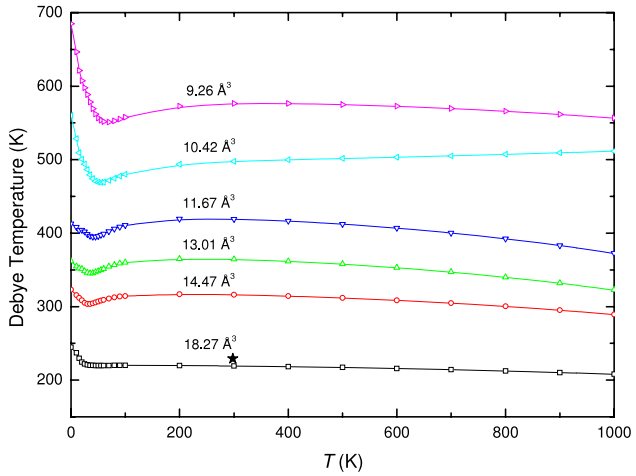

Figure 17. Debye temperature $\Theta_D(T)$ as a function of temperature at different volumes. The filled star is experimental datum at 298 K and 1 atm from [38].

the quasiharmonic approach, the interactions among phonons and the interactions between electrons and phonons are not considered. Comparing our thermal expansion results with experiment (figure 9), one sees that at ambient pressure the valid range of the QHA for Ta is considerably larger, i.e. from

0 to 1700 K. At ambient pressure and above 1700 K, the higher-order anharmonicity must be considered completely. As far as the calculation of anharmonicity of the solid and even the liquid is concerned, Alfè *et al* have done plenty of excellent work using the thermodynamic integration technique [8, 28, 39]. While, in this work, the obtained properties are reliable below 1700 K at ambient pressure, in the temperature range from 1700 K to melting point it is questionable, and beyond the melting point the results are nonphysical. At high pressures, pressure strengthens the bonding among atoms and lowers the vibrational distances of atoms from their equilibrium positions, so the valid range of the QHA can be extended to higher temperature, e.g. the Hugoniot properties are well reproduced up to 150 GPa and around 3000 K (figure 8 inset). The Debye temperature of Ta at 0 GPa (18.47 $Å^3$) is 220 K and the highest valid temperature is about $7.7\Theta_D$. Similar conclusions have been drawn for thorium [40]. As shown in figure 17, Θ_D increases significantly as pressure increases (decrease of volume) and the highest valid temperature also increases with increasing pressure. By analyzing the Hugoniot curve and the Debye temperature at high pressure and temperature, we note the highest valid temperature may be still 6 or 7 times the Debye temperature at high pressure.

4. Conclusion

We employed the density functional perturbation theory (DFPT) to refine the lattice dynamical properties, thermal equation of state and thermodynamic properties of bcc Ta. The calculated phonon dispersion curve accords excellently with experiment. We also well reproduced the thermal EOS properties including isotherms, thermal pressure and Hugoniot properties. Thermodynamic properties are very important to extrapolate thermophysical properties to higher pressures and temperatures. The specific heats C_P and C_V are considerably improved in our work compared with those of Cohen and Gülseren. The thermodynamic Grüneisen parameter as a function of pressure and temperature was properly derived and the Grüneisen parameter we obtained at 0 K and 0 GPa is very close to the experimental zero-pressure room temperature value. Note that the QHA only includes a part of anharmonicity by allowing phonon frequencies to vary with crystal volume, but it ignores the change of electronic structure with increasing temperature and the effects on the lattice dynamical properties. Therefore, when the temperature is very high (6 or 7 times the Debye temperature) or close to the melting point, complete anharmonic effects should be considered in the calculations. However, the excellent agreement of our obtained thermal expansion and Hugoniot curves with experiments greatly verify the validity of the QHA at higher temperatures not close to the melting point. As it is known that pressure strengthens the bonding among atoms and then lowers the vibrational distances of atoms from their equilibrium positions, so the valid range of the QHA can be extended to higher temperature at high pressure.

Acknowledgments

The authors would like to thank Professor Alfè for valuable discussions. We also acknowledge the support by the National Natural Science Foundation of China under grant no. 10776029, the NSAF under grant no. 10776022, the National Key Laboratory Fund for Shock Wave and Detonation Physics Research under grant no. 9140C6702030802 and the Science Foundation of China Academy of Engineering Physics under grant no. 2007B09002.

References

[1] Cohen R E and Gülseren O 2001 *Phys. Rev.* B **63** 224101
[2] Cynn H and Yoo C 1999 *Phys. Rev.* B **59** 8526
[3] Dewaele A, Loubeyre P and Mezouar M 2004 *Phys. Rev.* B **70** 094112
[4] Chijioke A D, Nellis W J and Silvera I F 2005 *J. Appl. Phys.* **98** 073526
[5] Orlikowski D, Söderlind P and Moriarty J A 2006 *Phys. Rev.* B **74** 054109
[6] Bercegeay C and Bernard S 2005 *Phys. Rev.* B **72** 214101
[7] Foata-Prestavoine M, Robert G, Nadal M and Bernard S 2007 *Phys. Rev.* B **76** 104104
[8] Taioli S, Cazorla C, Gillan M J and Alfè D 2007 *Phys. Rev.* B **75** 214103
[9] Errandonea D 2005 *Physica* B **357** 356
Errandonea D, Schwager B, Ditz R, Gessmann C and Boehler R 2001 *Phys. Rev.* B **14** 132104
Luo S N and Swift D C 2007 *Physica* B **388** 139
Ross M, Errandonea D and Boehler R 2007 *Phys. Rev.* B **76** 184118
Verma A K, Rao R S and Godwal B K 2004 *J. Phys.: Condens. Matter* **16** 4799
Wang Y, Ahuja R and Johansson B 2001 *Phys. Rev.* B **65** 014104
[10] Errandonea D, Somayazulu M, Häusermann D and Mao H K 2003 *J. Phys.: Condens. Matter* **15** 7635
[11] Moriarty J A, Belak J F, Rudd R E, Soderlind P, Streitz F H and Yang L H 2002 *J. Phys.: Condens. Matter* **14** 2825
[12] Strachan A, Cagin T, Iseren O G, Mukherjee S, Cohen R E and Goddard W A III 2004 *Modelling Simul. Mater. Sci. Eng.* **12** S445
[13] Liu Z L, Cai L C, Chen X R and Jing F Q 2008 *Phys. Rev.* B **77** 024103
[14] Gannarelli C M S, Alfè D and Gillan M J 2005 *Phys. Earth Planet. Inter.* **152** 67
[15] Holmes N C, Moriarty J A, Gathers G R and Nellis W J 1989 *J. Appl. Phys.* **66** 2962
[16] Mitchell A C and Nellis W J 1981 *J. Appl. Phys.* **52** 3363
[17] Nellis W J, Mitchell A C and Young D A 2003 *J. Appl. Phys.* **93** 304
[18] Moriarty J A 1994 *Phys. Rev.* B **94** 12431
Soderlind P and Moriarty J A 1998 *Phys. Rev.* B **57** 10 340
[19] Mermin N D 1965 *Phys. Rev.* **137** A1441
[20] Sha X and Cohen R E 2006 *Phys. Rev.* B **73** 104303
[21] Tsuchiya T and Kawamura K 2002 *Phys. Rev.* B **66** 094115
[22] Baroni S, Giannozzi P and Testa A 1987 *Phys. Rev. Lett.* **58** 1861
Gonze X 1997 *Phys. Rev.* B **55** 10337
Gonze X and Lee C 1997 *Phys. Rev.* B **55** 10355
Zein E N 1984 *Sov. Phys.—Solid State* **26** 1825
[23] Baroni S, Gironcoli S d, Corso A D and Giannozzi P 2001 *Rev. Mod. Phys.* **73** 515
[24] Perdew J P, Burke K and Ernzerhof M 1996 *Phys. Rev. Lett.* **77** 3865
[25] Monkhorst H J and Pack J D 1976 *Phys. Rev.* B **13** 5188
[26] Woods A D B 1964 *Phys. Rev.* **136** A781
[27] Birch F 1978 *J. Geophys. Res.* **83** 1257
Birch F 1986 *J. Geophys. Res.* **91** 4949

[28] Alfè D, Price G D and Gillan M J 2001 *Phys. Rev.* B **64** 045123
[29] Anderson O L and Isaak D G 2002 *Phys. Earth Planet. Inter.* **131** 19
[30] Isaak D G, Anderson O L and Goto T 1989 *Phys. Chem. Minerals* **16** 704
[31] Karki B B 2000 *Am. Mineral.* **85** 1447
[32] Jackson I and Rigden S M 1996 *Phys. Earth Planet. Inter.* **96** 85
[33] Marsh S P 1979 *Los Alamos Shock Hugoniot Data* (Berkeley, CA: University of California Press)
Krupnikov K K, Bakanova A A, Brazhnik M I and Trunin R F 1963 *Sov. Phys.—Dokl.* **8** 205
[34] Wang Y, Chen D Q and Zhang X W 2000 *Phys. Rev. Lett.* **84** 3220
[35] Touloukian Y S, Kirby R K, Taylor R E and Lee T Y R 1977 *Thermophysical Properties of Matter* (New York: IFI/Plenum)
[36] Edwards J W, Speiser R and Johnston H L 1951 *J. Appl. Phys.* **22** 424
[37] Grigoriev I S and Meilikhov E Z 1997 *Handbook of Physical Quantities* (New York: CRC Press)
Milošević N D, Vuković G S, Pavičić D Z and Maglić K D 1999 *Int. J. Thermophys.* **20** 1129
Kelley K K 1940 *J. Chem. Phys.* **8** 316
Kulish A A and Philippov L P 1978 *Teplofiz. Vys. Temp.* **16** 602
Hoch M and Jonhston H L 1961 *J. Chem. Phys.* **65** 855
[38] Guillermet A F and Grimvall G 1989 *Phys. Rev.* B **40** 1521
[39] Alfè D, Gillan M J and Price G D 1999 *Nature* **401** 462
Alfè D and Gillan M J 2003 *Phys. Rev.* B **68** 205212
Alfè D, Gillan M J and Price G D 2002 *Phys. Rev.* B **65** 165118
Vočadlo L and Alfè D 2002 *Phys. Rev.* B **65** 214105
Alfè D and Gillan M J 1998 *Phys. Rev.* B **58** 8248
Alfè D 2005 *Phys. Rev. Lett.* **94** 235701
Gillan M J, Alfè D, Brodholt J, Vočadlo L and Price G D 2006 *Rep. Prog. Phys.* **69** 2365
Alfè D, Gillan M J and Price G D 2000 *Nature* **405** 172
Alfè D, Price G D and Gillan M J 2004 *J. Phys. Chem. Solids* **65** 1573
Alfè D, Vočadlo L, Price G D and Gillan M J 2004 *J. Phys.: Condens. Matter* **16** S973
[40] Bouchet J, Jollet F and Zérah G 2006 *Phys. Rev.* B **74** 134304